Journal of Mines, Metals and Fuels, *71(12): 2520-2526; 2023. DOI: 10.18311/jmmf/2023/36244*

Print ISSN : 0022-2755

Journal of Mines, Metals and Fuels

Contents available at: *www.informaticsjournals.com/index.php/jmmf*

Role of Metal Nanoparticles in the Fabrication of Porous Silicon: A Material for Solar Cell Applications

Karanam Madhavi, G. Vijayakumar, N. Hanumantha Raju, K. S. Hemalatha and V. C. Veeranna Gowda*

Department of Physics, Maharani Cluster University, Bangalore - 560001, Karnataka, India; vcvgowda@gmail.com

Abstract

Metal-Assisted Chemical Etching method (MACE) has emerged as an effective tool to fabricate silicon nanostructures. This technique requires a catalytic mask that is commonly composed of a metal. In the present work, the role of Silver nanoparticles (AgNPs) in the etching mechanism of Porous Silicon (PS) is investigated by studying the effect of AgNP coverage on the surface porosity and the different properties of PS. XRD spectra consist of the two peaks corresponding to silicon and AgNPs respectively and the peak intensity of Ag decreased with an increase in etching time which indicates that as the etching time increases the dissolution of silver metal also increases. Thus, the pore depth depends on the dissolution of AgNP. The pore depth and porosity are calculated at different etching times by SEM analysis. It is observed that porosity is modifiable with the variation of AgNP coverage which in turn modifies the optical properties of PS. The porosity increased with the increase of etching time and the highest porosity obtained was 78% after 240 minutes. The refractive index of PS decreased with increasing porosity in the visible region. The variation of the refractive index results in the tuning of optical energy gap which is more essential in increasing the efficiency of solar cells.

Keywords: *Metal Nanoparticles, Porous Silicon, Porosity, Refractive Index*

1.0 Introduction

Metals play an important role in the fabrication of silicon nanostructures by the Metal-Assisted Chemical Etching method (MACE). In metal-assisted chemical etching, Metal Nano Particles (MNP) such as Platinum (Pt), Gold (Au), and Silver (Ag) can be practically used to assist the etching of Si for producing silicon nanostructures. A progressive move down in the dimensionality of semiconductors has been seen at the end of the last century in the form of quantum wells, quantum dots and quantum wires which are the key points for the development of nanoelectronics. Thus silicon (Si) which has been the most widely used semiconductor in the field of electronics is a fascinating option as the basic material for one-dimensional semiconductor structures, such as porous silicon, nanowires, and nanorods. The nanostructures of silicon have attracted much curiosity over the last few decades due to their distinctive structural, optical, mechanical, thermal, and electrical properties[1]. The Porous Silicon (PS) is one of the silicon nanostructures that has voids in the range of 4% to 95% and was first reported by Uhler in 1956. Due to the nano size and high surface ratio, PS has higher elasticity, visible photoluminescence, and direct band gap structure compared to bulk silicon[2]. Thus, PS has been under distinctive investigations in the last decade due to its wider applications in optoelectronic devices, and chemical and biochemical sensors[3-5]. Many

*Author for correspondence

methods have come up to fabricate PS materials, among which, the Metal-Assisted Chemical Etching (MACE) method is simple and cost-effective which is purely solution-based and produces a uniform porous layer on the silicon without the requirement of external biasing[6]. The MACE method is based on the deposition of noble metal nanoparticles which act as catalysts for the chemical etching process. The morphology of porous silicon depends on the type of noble metal used. The etch rate also depends on the type of noble metal. The shape of the noble metal influences the geometry of the porous silicon nanostructures. The potential to apply porous silicon in different applications results from optical and structural properties[7]. The optical properties of PS samples are determined by porosity, refractive index, and size of the pores.

In the present study, the influence of the AgNP coverage area on the etching process is studied through experimental evidence. We studied the correlation between AgNP coverage area and porosification through SEM analysis and the influence of etching time on the porosity on the optical properties of PS namely the refractive index, optical band gap energy and absorption coefficient. The porosity and pore size are determined by a geometrical approach and the value of the refractive index of PS at different etching times is calculated by using three effective medium methods Bruggeman approximation[8], Looyenga formula[9], and the Maxwell–Garnett mixing rule[10] measured the deviation from the reference value. The value of the refractive index with less deviation is used for further calculations.

2.0 Materials and Methods

2.1 Materials

The 3-inch p-type <100> single crystalline silicon wafers used in this study are with a resistivity of 1-10 Ω-cm. The annular grade silver nitrate ($AgNO_3$), hydrofluoric acid (48%), Nitric acid (HNO_3), hydrogen peroxide (H_2O_2), acetone, ammonia, and sulphuric acid (H_2SO_4) were used.

2.2 Synthesis and Fabrication of Porous Silicon

The RCA technique is used to clean silicon wafers[11]. After the removal of oxide on silicon by immersing it in the 5% HF solution, the silver nanoparticles accumulated on the silicon wafer by soaking it in the aqueous solution containing 0.005 M $AgNO_3$ and HF (4.8M) in the volume ratio of 1:1 for 40 seconds. The silver-deposited silicon wafer later soaking in the etching bath consists of 4.8M HF and 0.5M H_2O_2 for 60 minutes. The etched silicon is rinsed thoroughly with deionised water and then immersed in the 7.2M HNO_3 solution to remove the residual Ag nanoparticles. By immersing in the 5% HF solution, the oxide layer generated on the etched silicon due to the HNO_3 solution is eliminated[12]. Finally, the sample is completely cleaned with deionized water and dried by nitrogen blowing. The process is repeated for different etching times.

2.3 Characterization

All etching levels are carried out at room temperature. A scanning electron Microscope is used to examine the surface morphology. (JEOL, JSM-6330F). The crystallographic phase study is carried out using an X-ray diffractometer (Rigaku diffractometer). The CT-25C spectrometer was used to perform the optical absorption measurements. (JASCO), a 50-W halogen lamp, and a liquid-nitrogen-cooled Ge photodiode (Hamamatsu, B6175-05).

3.0 Results and Discussion

3.1 X-ray Diffraction Analysis

After the fabrication of PS, the X-Ray Diffraction (XRD) measurements were done to examine the grain size in PS material. Figure 1 depicts the XRD of PS at different etching times, which demonstrates the presence of two peaks at 69.19^0 and 69.41^0 for silicon and Ag respectively[13]. The peak intensity of Ag decreases as the etching time increases. This can be related to the fact that as the etching time increases, silver dissolution also increases. The increase in AgNP dissolution increases pore depth, which has been confirmed by SEM images as shown in Figure 2. The porous silicon XRD pattern exhibiting the preferred direction (100) indicates that the porous silicon has good crystalline quality[14]. Using Scherrer's formula, the average grain size, d, is determined from the obtained XRD data[15],

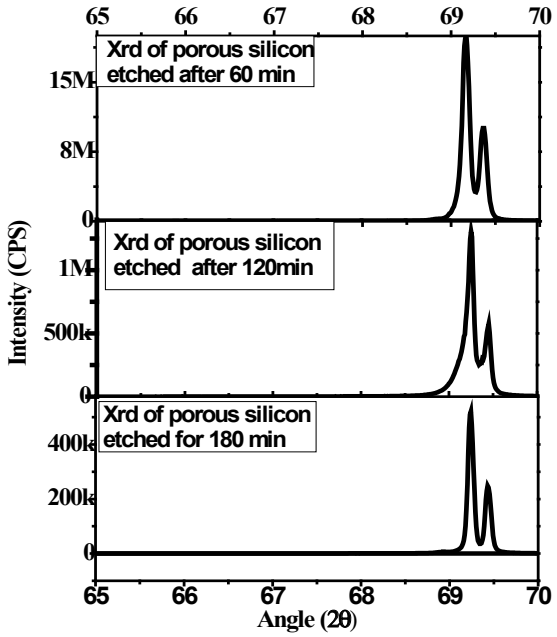

Figure 1. XRD patterns of porous silicon fabricated at different etching times.

$$d = \frac{0.9\lambda}{\beta cos\theta} \quad (1)$$

where *lambda is* the wavelength of X-rays beta is full-width half maxima (FWHM and theta is the Bragg's angle. The etching time, FWHM and grain size of PS are listed in Table 1.

3.2 SEM Analysis

Figure 2 shows the SEM images of silver deposition on a silicon wafer after exposure to a solution containing HF and $AgNO_3$. Figure 2 (a) shows the morphology of Ag nanoparticles loaded on the silicon wafer after 40 sec depositions in the above aqueous solution. The mean diameter of the Ag nanoparticle is 53.7 nm. Figure 2 (b) shows the plan view image of the porous silicon after etching the AgNP deposited silicon etching in solution HF-H_2O_2-H_2O for 60 min. The method of Ag nanoparticle deposition and the synthesis of PS is discussed explicitly in our previous work[16]. The generation of pores through

Table 1. XRD data of porous silicon at different etching time

Etching time (min)	2 (Degree)	FWHM(β) (Degrees)	Grain size (nm)
60	69.25	0.078	104.53
120	69.25	0.2738	72.79
180	69.24	0.1120	29.84

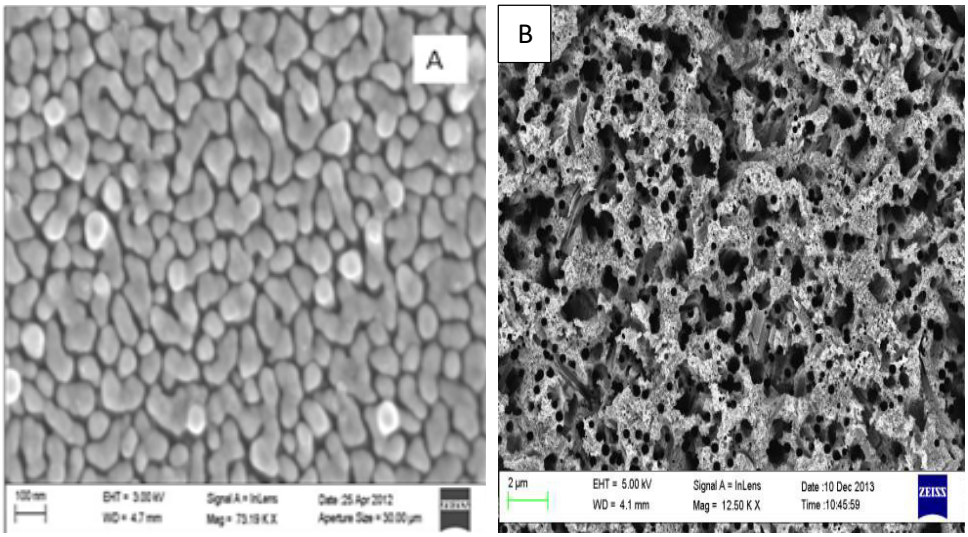

Figure 2. SEM images of **(a)** Silver nanoparticle (AgNP) deposition **(b)** pores on silicon after dissolution of Silver (Ag).

etching is possible through the reduction of H_2O_2 at the silver nanoparticles. A more AgNPs-covered area produces more porosification. Thus, the AgNP coverage area on silicon influences the formation of pores on the silicon. Since silicon below the AgNP dissolves most easily in the (100) direction, the pores preferably formed in the (100) direction and Ag nanoparticles sink in the same direction. The etching time is varied between 60 min to 240 min. It is observed that the average pore size increases from 0.23 μm to 0.4 μm and the distance between the pores varies between 0.3 μm to 0.7 μm with the increase of etching time. The porosity of PS samples was determined by a geometrical method using SEM analysis[17] and is given by,

$$P = \frac{\pi}{2} \times 1.732 \times \left[\frac{1}{1 \pm \frac{m}{d}}\right]^2 \quad (2)$$

where P is the porosity in percentage, d is the average pore size, and m is the distance between the pores. From the above equation, the porosity of the etched samples prepared for 60 min, 120 min, 180 min, and 240 min has been estimated as 20.12%, 22.19%, 41.48% and 78% respectively. Distance between the pores, pore size and the porosity values of PS at different etching times are listed in Table 2. Figure 3 shows the variation of porosity with etching time.

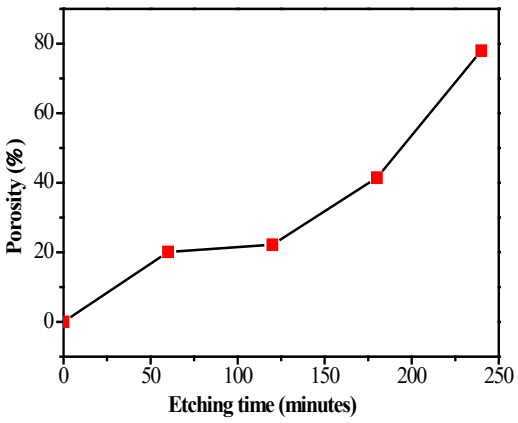

Figure 3. Variation of porosity with etching time.

3.3 Refractive Index Calculations

The Porous Silicon (PS) is a mixture of bulk silicon and voids. Thus, the index of refraction of PS depends on porosity and is expected to be lower than that of bulk silicon[17]. The effective medium approximations such as Looyenga, Maxwell Garnite and Braggmen equations were used to calculate the refractive index of PS. These approximation methods depend on the porosity and morphology of PS. We calculated the refractive index of PS by three EMA methods using the porosity values at different etching times.

(a) Looyenga Equation

$$\eta_{ps}^{2/3} = (1-p)\eta_{ps}^{2/3} + P\eta_{air}^{2/3} \quad (3)$$

(b) Maxwell Garnite Equation

$$(1-P)\frac{\eta_s^2 - \eta_{air}^2}{\eta_s^2 + \eta_{air}^2} = \frac{\eta_s^2 - \eta_{air}^2}{\eta_s^2 + \eta_{air}^2} \quad (4)$$

(c) Braggmen Equation

$$\eta_{ps} = 0.5\left[\left(3P(1-\eta_{Si}^2) + (2\eta_{Si}^2 - 1) + (3P(1-\eta_{Si}^2) + (2\eta_{Si}^2 - 1)\right)^2 + 8\eta_{Si}^2\right)\right]^{0.5} \quad (5)$$

Where η_{ps}, η_s and η_{air} are refractive index of PS, the refractive index of bulk silicon and refractive index of air respectively. The refractive index of PS is calculated

Table 2. Porosity values of porous silicon at different etching times

Etching time (min)	Distance between the pores (cm)	Pore size (cm)	Porosity (%)
60	0.307	0.23	10
120	1	0.3	22.19
180	0.62	0.3	41.48
240	1.66	0.6	78

Table 3. Refractive Index of porous silicon

Porosity %	Refractive Index (η)			Reference value from the reports
	Bruggmen Method	Maxwell –Garnett Method	Looyenga Method	
10%	3.15	2.85	3.20	2.91[17]
22.19%	2.81	2.38	2.90	2.84[17]
41.48%	2.31	1.75	2.19	2.38[17]
78%	1.43	1.24	1.33	1.44[20]

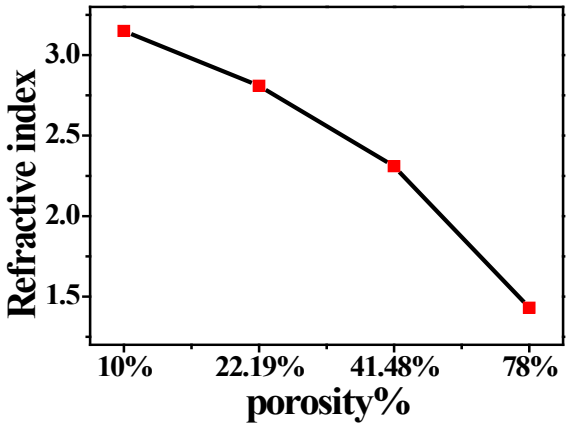

Figure 4. Variation of refractive index of PS with porosity.

as a function of porosity by using the above models and compared with the literature value shown in Table 3. The calculations of the refractive index are in good agreement with the values reported earlier[18] and the refractive index of PS is decreased with the increase of porosity. It is found that the refractive index calculated by the Bruggeman method shows less deviation from the reference value compared to the other two methods. Figure 4 shows the variation of refractive index with porosity.

3.4 Absorption Coefficient of Porous Silicon

The absorption coefficient of PS is determined from the equation given below[19],

$$\alpha = \frac{2.303 \times A}{t} /m \qquad (6)$$

where α is the absorption coefficient of porous silicon, A is the absorbance and t is the thickness of porous silicon.

The absorption coefficient (α) at different etching times is measured at the wavelength, λ = 650 nm, we chose it to study the optical properties of porous silicon at a specific wavelength. From the calculations, it is found that porous silicon exhibits the lowest absorption coefficient for an etching time of 240 min which exhibited the highest porosity of 78%. This result is in good agreement with the values reported earlier, that increase in porosity produces a blue shift in absorption coefficient[20]. The variation of the absorption coefficient with porosity is shown in Figure 5.

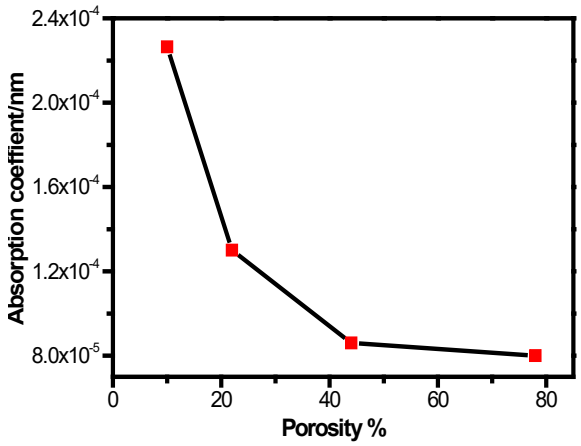

Figure 5. Variation of absorption coefficient with porosity.

3.5 Optical Band Gap Energy of Porous Silicon

The optical band gap energy E_g of PS at different etching times is determined from the theoretical Equation

$$E_g = \frac{\eta_{ps} - a}{b} \qquad (7)$$

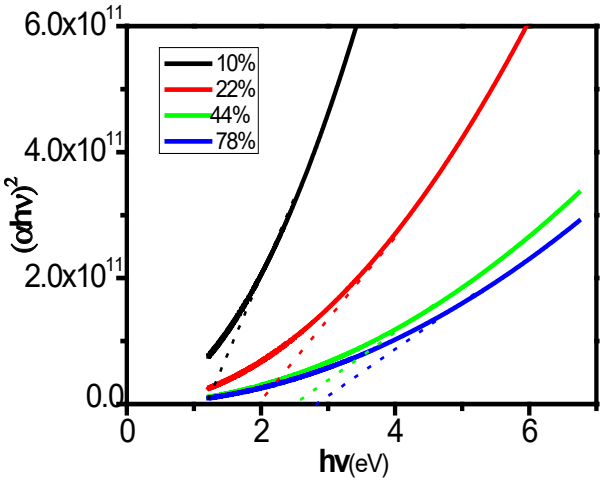

Figure 6. The variation of $(\alpha h\nu)^2$ verses hν.

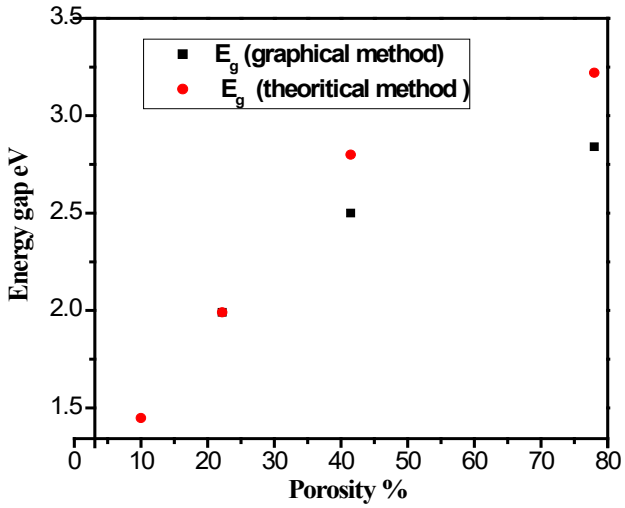

Figure 7. Variation of optical energy gap with porosity.

Table 4. Optical band gap energy (E_g) of porous silicon at different etching times

Etching time (min)	$\eta_P{}^S$	Porosity (%)	Absorption coefficient	E_g (eV) (Graphical)	E_g (eV) (Theoretical)
60	3.15	10	0.000226	1.23	1.448
120	2.81	22.19	0.000130	1.99	1.99
180	2.31	41.48	0.000086	2.50	2.80
240	1.43	78	0.000080	2.84	3.22

where a = 4.084, b = -0.62eV^{-1} and η_{ps} is the index of refraction of PS[21]. It is found that the optical band gap energy is increased with the decrease of the refractive index.

We also calculated E_g by graphical method. PS is direct band gap material which was verified by its photoluminescence properties reported in our previous study[16]. Thus, a graph is plotted between $(\alpha h\nu)^2$ verses graph and is shown in Figure 6. The extrapolation of the curve obtained from Figure 6 on the photon energy (hν) axis with zero absorption gives the bandgap energy E_g [22]. The energy gap increased with the increase of porosity. The values of E_g are calculated from the graphical method and theoretical method. Table 4 gives a comparison of E_g values at different etching times. It is found that they are in good agreement as shown in Figure 7.

4.0 Conclusion

Various porous silicon samples are prepared by varying the etching time and studying the correlation between silver metal nanoparticle coverage area and porosity. X-ray diffraction analysis was carried out to determine the crystalline size of porous silicon and found that the lowest grain size obtained was 29.84 nm. The porosity of porous silicon was determined at different etching times by geometrical method using plane view SEM images. The optical properties such as refractive index, absorption coefficient and energy gap of porous silicon were calculated. The refractive index of porous silicon is measured at different etching times by effective media approximation methods. The refractive index is found to decrease with the increase of porosity in three EMA methods. Absorption coefficient is calculated

using absorbance and it is decreased with the increase of porosity which is in good agreement with previous reports. Optical band gap energy was measured from verses graph for PS samples at different porosities for direct allowed transitions and from the theoretical equation and it was observed that band gap energy values were almost the same from the theoretical and graphical method which increased from 1.22 eV to 2.84 eV with increasing porosity. Thus, porosity enhancement is important in tuning the optical properties such as decrease of reflectance, increase of absorbance and widening the energy gap which are most essential for the use in solar cell applications.

5.0 References

1. Bisi O, Ossicini S, Pavesi L. Porous silicon: A quantum sponge structure for silicon-based optoelectronics. Surf Sci Rep. 2000; 38:1-126. https://doi.org/10.1016/S0167-5729(99)00012-6
2. Lin VSY, Motesharei K, Dancil KPS, Sailor MJ, Ghadiri MR. A porous silicon-based optical interferometric biosensor. Science. 1997; 278:840-3. https://doi.org/10.1126/science.278.5339.840 PMid:9346478
3. Canham LT. Silicon quantum wire array fabrication by electrochemical and chemical dissolution of wafers. Appl Phys Lett. 1990; 57:1046-8. https://doi.org/10.1063/1.103561
4. Sailor MJ, Lee EJ. Surface chemistry of luminescent silicon nanocrystallites. Adv Mater. 1997; 9:783-93. https://doi.org/10.1002/adma.19970091004
5. Canham LT. Bioactive silicon structure fabrication through nano etching techniques. Adv Mater. 1995; 7:1033-7. https://doi.org/10.1002/adma.19950071215
6. Yae S, Kawamoto Y, Tanaka H, Fukumuro N. Formation of porous silicon by metal particle enhanced chemical etching in HF solution and its application for efficient solar cells. Electrochem Commun. 2003; 5:632-6. https://doi.org/10.1016/S1388-2481(03)00146-2
7. Sohn H. Handbook of porous silicon, springer. Switzerland; 2014. p. 1-12. https://doi.org/10.1007/978-3-319-04508-5_25-1
8. Bruggeman DAG. Effective medium approximation for nonlinear conductivity of a composite medium. Ann Phys. 1935; 24:636-79. https://doi.org/10.1002/andp.19354160705
9. Looyenga H. Dielectric constants of heterogeneous mixtures. Physica. 1965; 31:401-6. https://doi.org/10.1016/0031-8914(65)90045-5
10. Garnett JCM. Colours in metal glasses, metallic films, and metallic solutions. II. Philos Trans R Soc Lond Soc. 1904; 203:385-420. https://doi.org/10.1098/rsta.1904.0024
11. Tans SJ, Verschueren ARM and Dekker C. Room-temperature transistor based on a single carbon nanotube. Nature. 1998; 393:49-52. https://doi.org/10.1038/29954
12. Kolasinski KW, Gogola JW. Rational design of etchants for electroless porous silicon formation. ECS Trans. 2011; 33:23-8. https://doi.org/10.1149/1.3553152
13. Hazra P, Jit S. An in-house approach for fabrication of silicon nanowire arrays using electroless metal deposition and etching method. Int J Surf Sci Eng. 2013; 7:285-94. https://doi.org/10.1504/IJSURFSE.2013.056439
14. Vinila VS, Jacob R, Mony A, Nair HG. X-ray diffraction analysis of nanocrystalline ceramic PbBaTiO3. Sci Res. 2014; 3:57-65. https://doi.org/10.4236/csta.2014.33007
15. Peter LM, Blackwood DJ, Pons S. *In situ* characterization of the illuminated silicon-electrolyte interface by Fourier-transform infrared spectroscopy. Phys Rev Lett. 1989; 62:308-11. https://doi.org/10.1103/PhysRevLett.62.308 PMid:10040199
16. Karanam M, Rao MG, Shaik H, Suvarna PR. Study of the properties of the porous silicon synthesized by Ag-assisted chemical etching. Int Lett chem Phys Astron. 2016; 71:40-8. https://doi.org/10.18052/www.scipress.com/ILCPA.71.40
17. Lakshmipriya V, Jeyakumaran N, Kumaran P. Structural properties of porous silicon layers - Influence of etching time. Int J Chemtech Res. 2014; 6:5261-4.
18. Alfeel F, Awad F, Qamar F. Tunable optical properties of porous silicon. J Basic Sci. 2014; 30:41-51.
19. Verhoeven JW. Glossary of terms used in photochemistry. Pure Appl Chem. 1996; 68:2223-86. https://doi.org/10.1351/pac199668122223
20. Mortezaali A, Sani RS, Jooni JF. Correlation between porosity of porous silicon and optoelectronic properties. J Non-oxide Glasses. 2009; 1:293-9.
21. Ravindra NM, Auluck S, Srivastava VK. On the Penn gap in semiconductors. Phy Status Solidi b. 1979; 93:155-60. https://doi.org/10.1002/pssb.2220930257
22. Kenny N, Kannewurf CR, Whitmore DH. Optical absorption coefficients of vanadium pentoxide single crystals. J Phys Chem Solids. 1996; 27:1237-46. https://doi.org/10.1016/0022-3697(66)90007-2